Methods of Imaging Articular Cartilage Under Shear

A Thesis

presented to

the Faculty of the Graduate School

at the University of Missouri

In Partial Fulfillment

of the Requirements for the Degree

Master of Science

By

Charles Jacoby

Dr. Ferris Pfeiffer, Thesis Advisor

May 2019

The undersigned, appointed by the dean of the Graduate School, have examined the Thesis entitled

Methods for Imaging Articular Cartilage
Under Shear

presented by Charles Jacoby,
a candidate for the degree of Master of Bioengineering
and hereby certify that, in their opinion, it is worthy of acceptance.

Professor Ferris Pfeiffer

Professor Gang Yao

Professor Aaron Stoker

Acknowledgments

I would like to thank my advising professor Dr. Ferris Pfeiffer for all the help and support he provided. I would also like to thank Dr. Gang Yao, Mohammadreza Ravanfar, Dr. Stoker, and G. Ellison whose provide invaluable assistance.

Table of Contents

List of Figures and Tables

Abstract

Characterizing both the structure of articular cartilage, and its biomechanical properties is key to gaining a full understanding of how the tissue functions. Articular cartilage is an inhomogeneous tissue with a depth dependent functional structures. This results in anisotropic depth dependent mechanical properties, which help this tissue deal with a harsh mechanical environment. Collagen fibers orientation plays an important role in the significant depth dependent functional traits of articular cartilage. Distinguishing the structural regions of articular cartilage, and relating that to the depth dependent mechanical properties of the tissue, could lead to a significant increase in our understanding of the relationship between structure and function for articular cartilage.

Chapter 1: Purpose and Significance

1. Introduction

There are numerous studies that have evaluated the complex biomechanical properties of articular cartilage (Van C. Mow, Ateshian, & Spilker, 1993). Articular cartilage is versatile and plays an important physiological role. It is able to absorb and transmit forces acting on it, and provide a low friction surface at points of articulation in the body. For the tibiofemoral joint, shown in Figure 1.1, a common force the articular cartilage experiences is compression (Julkunen et al., 2013). Although, the knee also undergoes rotational and translation movements that create shear stress at the point of articulation (Shenoy et al., 2013). This is demonstrated by the six degrees of

Figure 1.1 *An anatomical representation of the tibiofemoral joint. (Cartilage of the Knee [Online image]. (2017).Retrieved September 15, 2018.(https://myhealth.alberta.ca/Health/Pages/conditions.aspx?hwid=tp13046)*

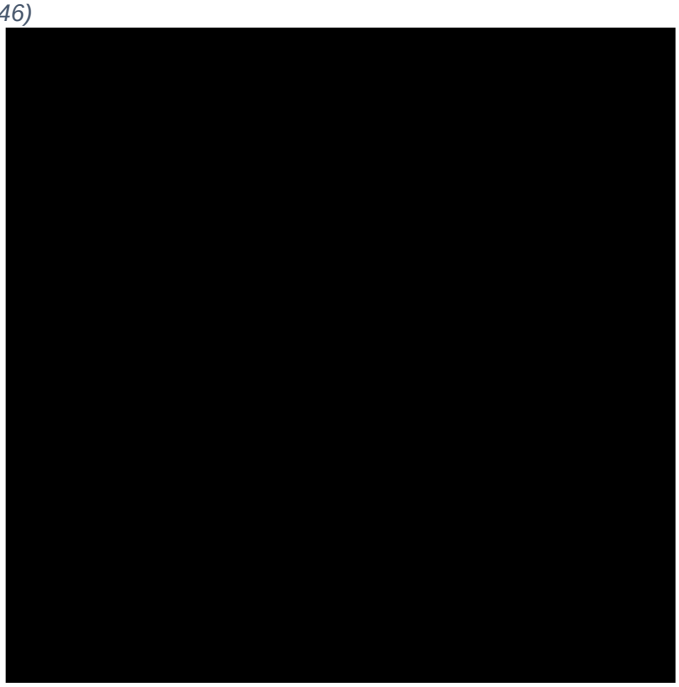

Figure 1.2 *Diagram showing the degrees of freedom of the tibiofemoral joint and the anatomical terms for each movement. Image from (Shenoy, Pastides, & Nathwani, 2013, p. 364)*

freedom shown in figure 1.2. Articular cartilage needs to absorb and/or transmit compressive, shear, and other forces being applied at the point of articulation (Sophia Fox, Bedi, & Rodeo, 2009). To accomplish this, articular cartilage has an anisotropic structure with functional regions to absorb and transmit different forces further discussed in section 1.1.1 and 1.1.2.

One of the key attributes of this functionality is the collagen fiber orientation in different regions (Silverberg et al., 2014). However, both supraphysiologic compression and shear forces degrade articular cartilage under static, cyclical, or large traumatic loads, although the rate of degradation varies with force and load conditions (Julkunen et al., 2013). Articular cartilage is an avascular tissue with a poor regenerative ability. Once damaged the tissue, the tissue has not been shown to heal itself, and articular cartilage is typically replaced with a fibrocartilage that has a different biochemical composition and structure, resulting in reduced biomechanical architecture (Hunziker, 2002). The progressive degeneration and loss of articular cartilage the hallmark of the disease osteoarthritis (OA), which is further discussed in section 1.2.

Henak, Anderson, & Weiss disscus how joint contact forces relate to OA. It is their perspective that most experiments and simulations point to shear force being the mechanism that most commonly leads to failure and degradation in knee articular cartilage. An increase in shear forces acting on the articular surface can be due to a decrease in joint stability caused by ligament injury or knee surgery, lesions, a traumatic loading event, or other circumstances (Henak, Anderson, & Weiss, 2013). One hypothesis is that even slight degradation at the

articular surface can have a large effect on the progression of OA (Teeple et al., 2007). The goal of this research is to gain insight into the structural and functional traits of articular cartilage under shear forces, and the importance of collagen fiber orientation.

1.1 Articular cartilage

1.1.1 Physiology

Articular cartilage is a connective tissue that exist at the points of contact between bones in diarthrodial joints (Sophia Fox et al., 2009). It is key to creating a surface with a low coefficient of friction for articulation; though the coefficient of friction varies along the articular surface in proportion to the load born in the region (Chan, Neu, Komvopoulos, & Reddi, 2011). It is subjected to large amounts of force under a variety of loading conditions (Van C Mow & Guo, 2002), and it has a complex extracellular matrix (ECM) structure that allows to perform its physiological role in a severe biomechanical environment.

Articular cartilage is a porous biphasic tissue that contains up to 80% water by mass under physiological conditions. This water, or extracellular fluid, exists within a framework of macromolecules called the extracellular matrix (ECM), and is vital to the tissue's biomechanical function (Chan et al., 2011). The other ECM constituents include collagen fibers (15-30%), proteoglycans (4-7%), chondrocytes (1%), and other proteins (J. Buckwalter & Mankin, 1998).

Articular cartilage is a hypocellular tissue, and chondrocytes are the only cell type found within normal tissue (Hwang & Kim, 2015). The chondrocyte

varies in size and shape in a tissue depth dependent manner, and they are responsible for producing and maintaining the ECM (Jadin et al., 2005; M. Wong, Wuethrich, Eggli, & Hunziker, 1996). Chondrocytes respond to a variety of physiological stimuli, and can repair/modulate the ECM in response to these stimuli (Hunziker, 2002). However, chondrocytes have a very limited ability to proliferate that decrease with age, which contributes to the limited ability of cartilage to rejuvenate (Sophia Fox et al., 2009).

Each chondrocyte is surrounded by a layer with a higher percentage proteoglycans that contains type VI and type II collagen forming a mesh-like capsule. This is referred to as the pericellular matrix (PCM) (McLeod, Wilusz, & Guilak, 2013, p. 587). The transitional region between the PCM and ECM is a structurally distinct matrix of collagen fibers, which is likely meant to help protect the cell (Darling, Wilusz, Bolognesi, Zauscher, & Guilak, 2010). The PCM and transitional region have different biomechanical properties (Torzilli, Deng, & Ramcharan, 2006). The variance in the cellularity within the ECM contributes to the anisotropic properties, which in part is due to the PCM and transitional region around each cell (McLeod et al., 2013).

Type II collagen makes up 90-95% of the collagen in articular cartilage, but Types I, IV, V, VI, IX, and XI are also present (Sophia Fox et al., 2009). The other types of collagen support and complement Type II collagen. Types IX and XI are integrated with type II to form an interwoven structure that has a high tensile strength (Temenoff & Mikos, 2000). The previously mentioned PCM can be distinguished by the presence of Type VI collagen, which helps form the

mesh-like capsule (Poole, Ayad, & Schofield, 1988). The presence of certain types of collagen, and the orientation of the fibers characterize the ECM region (J. Buckwalter & Mankin, 1998). The impact of this regionalized structure on the biomechanical properties is expanded upon in section 1.1.2.

As shown in Figure 1.3, articular cartilage is organized into regions that are distinguished by cellular organization and morphology (Figure 1.3A), proteoglycan concentration, and collagen fiber orientation (Figure 1.3B) (Sophia Fox et al., 2009). In figure 1.3A, at the bottom of the articular cartilage is a region of calcified bone with a tidemark that is the demarcation between the cartilage and bone. The deep zone comprises 30-40% of the thickness. Next is the middle zone or transitional zone, which occupies about 40-60% of the thickness. Last, the superficial zone or tangential zone (STZ), which includes the region from the articular surface to a depth of 10%-20% of the overall cartilage thickness (J. A. Buckwalter, Mow, & Ratcliffe, 1994).

Figure 1.3 *Schematic showing the different regions of articular cartilage. A. Shows how the distribution and shape of chondrocytes varies at different depths. B. Shows collagen fiber orientation in the different zones. Image from(J. A. Buckwalter et al., 1994, p. 193)*

1.1.2 Region Structure and Mechanical Properties

Each zone found in articular cartilage has a distinct physical makeup, which in turn creates unique mechanical and functional properties (B. L. Wong & Sah, 2010). One important quality in each zone is collagen fiber orientation. This is illustrated in Figure 1.3 B. Collagen have a supramolecular structure that give them a great deal of tensile strength and stability. Figure 1.4 shows the structure of the collagen fiber that allows it to resist tension or compression. The helical structure of the collagen fiber must be oriented so the force is elongating or compressing the helix (Gelse et al., 2003). This is why the fiber orientation in each zone of articular cartilage is important to its physiological function.

Figure 1.4 *Represents the helical molecular structure of collagen. Image from (Gelse, Pöschl, & Aigner, 2003, p. 1534)*

Figure 1.3 B illustrates how the collagen fiber orientation varies through the depth of the cartilage tissue. The deep zone is characterized by collagen fibers that run perpendicular to the articular surface. They are typically organized

into stacked columns to help provide resistance to compression (J. A. Buckwalter et al., 1994). The collagen fibers of this region tend to have the largest diameter, and extend down to the tidemark (Temenoff & Mikos, 2000). The deep zone also tends to have the highest proteoglycan concentration, and the lowest water concentration (J. Buckwalter & Mankin, 1998). The chondrocytes in this zone are round, and are roughly 10 times synthetically active than their superficial zone counterparts (M. Wong et al., 1996).

The middle zone has more water and collagen than the deep zone, but less than the superficial zone. The fiber orientation in the middle the zone is more random than the other zones (Temenoff & Mikos, 2000). Also, the middle zone contains a mixture of the chondrocyte morphologies found in the superficial and deep zones (M. Wong et al., 1996). Based on these traits the middle zone represents the progression from the superficial to the deep zone. This may be why the middle zone is sometimes referred to as the transitional zone.

The superficial zone is the thinnest zone with the highest concentrations of collagen and water (J. Buckwalter & Mankin, 1998; Temenoff & Mikos, 2000). Chondrocytes in the superficial zone tend to be smaller, denser, flattened lengthwise to the articular surface (Mansfield, Bell, & Winlove, 2015). The collagen fibers in the superficial zone are oriented so the long helical structure (Figure 1.4) is parallel to the articular surface (Figure 1.3 B). An acellular layer at the articular cartilage surface contributes to the high concentration of collagen fibers in the superficial zone (J. Buckwalter & Mankin, 1998). This acellular layer is predominantly collagen and is also referred to as the lamina splendens

(Rexwinkle, Hunt, & Pfeiffer, 2017). The high concentration of collagen fibers in this layer leads to high tensile strength, and the parallel orientation of the fibers resist shear forces (Temenoff & Mikos, 2000). The lamina splendens is thought to have frictional properties that are vital to the function of the articular cartilage (Rexwinkle et al., 2017).

As a whole the ECM displays viscoelastic properties (Neu, Komvopoulos, & Reddi, 2008). This can be largely attributed the frictional drag of extracellular fluid as it flows through the porous matrix during displacement. These viscoelastic properties are explored during biomechanical testing including but not limited to load relaxation, creep, and hysteresis (Neu et al., 2008).

1.2 Osteoarthritis

1.2.1 Impact of OA

Osteoarthritis (OA) is a joint disease that results from the degradation of articular cartilage. Symptomatic OA is characterized by joint pain, inflammation, and stiffness that can be debilitating (Pritzker et al., 2006). An estimated 27 million Americans over the age of 25 are living with OA. OA is most commonly found in the knee, hip, neck, lower back, and finger joints (Vina & Kwoh, 2018; Zhang & Jordan, 2010).

Perhaps the most debilitating and costly forms of OA is in the lower limbs. A Global Burden of Disease study tracked data from 15 countries on the common disability causing diseases (Djalalinia et al., 2017). The metric they used was years lived with disability (YLD). OA was the 9th and 8th leading cause for YLD

for men and women respectively. Of these cases OA of the knee was the leading cause followed by the hip (Djalalinia et al., 2017). Based on data from the National Health Interview Survey there are 14 million Americans living with knee OA as of 2016. It was also estimated that the annual cost for one American to manage and treat of OA is $1,442 to $21,335 (Vina & Kwoh, 2018). The total burden annually on the EU could be as high as €408 to €817 billion/year ($478.93 to $959.04 billion /year) and €350 to €700 billion/year ($410.85 to $821.69 billion/year) for total and direct costs, respectively (Salmon et al., 2016, p. 6). The cost is in large part due to the OA often leading to surgical intervention such as total knee and hip replacement, which is $1,797 to $12,093 for knee and from $2,392 to $12,651 for hip (Salmon et al., 2016, p. 5). The significant effect on patient's quality of life and the economic burden associated with OA are important factors driving the pursuit of OA research aimed at developing novel treatment strategies for OA. Additionally, research to develop novel diagnostic and prognostic methodologies aimed at earlier detection and determination of disease development and progression should continue to be pursued.

1.2.2 Risk Factors for OA

There are a number of factors that can increase the risk of OA development. Systematic factors include age, genetics, gender/hormones, ethnicity, and congenital/developmental disorders. Because the development of OA is often multifactorial, there is no single measure to decrease risk (Vina & Kwoh, 2018; Zhang & Jordan, 2010).

Environmental factors such as diet, obesity, injury, surgery, occupation, and physical activities can all play a role in development of OA (Vina & Kwoh, 2018; Zhang & Jordan, 2010). Because the development of OA is often multifactorial, there is no single measure to decrease risk (Anderson et al., 2011; Lohmander, Östenberg, Englund, & Roos, 2004; Rasmussen, 1973; Vina & Kwoh, 2018; Zhang & Jordan, 2010).

However, understanding how these factors affect the articular cartilage and drive the changes in tissue biochemical, cellular, and biomechanical properties may lead to improved preventative and treatment strategies for OA clinically.

Chapter 2: Review of Literature

2.1 Articular Cartilage Biomechanical Testing

2.1.1 Articular Cartilage Samples

Articular cartilage is an avascular tissue (Temenoff & Mikos, 2000). Presumably, the lack of blood supply during *in vitro* testing is not as impactful as it would be for vascular tissue. When articular cartilage is removed from a synovial fluid-lubricated environment, a phosphate buffer saline (PBS) solution is often used to better approximate physiological conditions. However, the use of PBS has been shown to increase boundary mode friction when compared to synovial fluid (Schmidt, Gastelum, Nguyen, Schumacher, & Sah, 2007). Additionally, proteinase inhibitors in synovial fluid or PBS are used during storage to prevent further degradation of collagen fibers and proteoglycans, thereby preserving the extracellular matrix (Sun, 2010).

Biomechanical testing of articular cartilage is a vital area of research, and a variety of samples is used for experimentation. There is significant variation among samples for *in vitro* testing of human articular cartilage associated with the knee (from the femoral condyle or the tibial plateau). In some studies, the human patellofemoral joint is left relatively intact in an attempt to better understand its function as a whole (Guterl et al., 2009; Lee, Gerken, Glaser, Kim, & Anzel, 1997). This is accomplished by sectioning the knee proximal to the femur and distal to the tibia. The skin and musculature are stripped off as shown in Figure 2.1. The remaining portions of the femur and tibia, above each epiphysis, allow for fixation to the testing apparatus.

Application of the desired mechanical strain ensues, while leaving the articular capsule relatively intact (Lee et al., 1997).

With this method, it can be difficult to image the tissue during displacement, as it is not exposed. This leads to a reliance on mechanical data.

Another method of simulating the tibiofemoral joint under physiological conditions is to bisect both the femur and the tibia along the midsagittal line to make the point of contact between the two articular surfaces more visible (Guterl et al., 2009). The tibiofemoral joint is comprised of two chondral surfaces held together by muscle and ligament shown in Figure 2.1. With the joint no longer held together by a complete system of ligaments a fixation method must be used to keep the samples in an approximate anatomical position such that the appropriate regions interact.

Figure 2.1 *Visualization of the system of ligaments that support the tibiofemoral joint. Knee Joint [Online image]. (2018).Retrieved September 12, 2018. http://teachmeanatomy.info/lower-limb/joints/the-knee-joint/*

The most commonly used samples in articular cartilage biomechanics research are osteochondral cores. These explants are taken from the articular surface down to the calcified bone to include all the zones of the articular cartilage and a section of the bone (see Figure 1.3 B). A cylindrical biopsy punch is used, resulting in a cylindrical osteochondral core. In many studies, the cylindrical osteochondral cores are then bisected into hemi-cylinders. Images of the flat bisected surface are well-suited for tracking of reference points to quantify displacement.

Robinson (2016) started with a cylindrical osteochondral core 5 mm in diameter. A smaller concentric explant, 3 mm in diameter, was taken and used for mechanical testing to fins coefficients associated with the shear modulus. The outer ring was cut into thin cross-sections for histological analyses of the same relative region as the 3 mm cylindrical explant (Robinson et al., 2016).

2.2 Osteoarthritis Grading and Precursors

Articular cartilage is an avascular tissue and does not regenerate. Therefore, treatment of osteoarthritis would greatly benefit from advances in early detection, before serious degradation of the tissue occurs. Common objectives in this research area are to improve models and metrics for degradation, and to develop early stage indicators. One clear metric of articular cartilage degradation is degree of fibrillation characterized by the softening of the articular surface and exposed groups of collagen fibrils. This hallmark of OA was written about as far back as 1949 (Bennett, 1942; Meachim, Ghadially, & Collins, 1965).

The Pond-Nuki model is frequently referred to in OA research (Pond & Nuki, 1973). This model characterizes OA in canine articular cartilage. In this study, a large number of dogs had the anterior cruciate ligament ruptured on one hind leg, while leaving the other as a control. The ruptured ligament led to continual break down of the articular cartilage in the affected knee, as revealed by euthanization and dissection during points in the progression of OA. The surface of the affected knee and the control were observed using a scanning

electron microscope. OA progression was correlated with the varying degree of fibrillation, as well as the destruction of the acellular zone at the articular surface. The degree of fibrillation and the destruction of the acellular zone is commonly used to evaluate degradation of in vitro samples.

One histological method used to grade the progression of OA in samples is the Mankin score (Mankin & Lippiello, 1970). The Mankin Score characterizes articular cartilage samples based on structural abnormalities, tidemark integrity, cell population, and Safranin-O stain distribution. A modification of this scoring system is referred to as the histologic/histochemical grading system (HHGS) (Ostergaard, Petersen, Andersen, Bendtzen, & Salter, 1997). Lorenz (2004) also used a version of the Mankin score in combination with gene expression analysis to better understand the health of articular cartilage (Lorenz, Wenz, Ivancic, Steck, & Richter, 2004). The Osteoarthritis Research Society International (OARSI) osteoarthritis cartilage histopathology assessment system is based on some of the previously mentioned OA grading methods. The goal of the OARSI research team was to improve the simplicity, utility, scalability, extendibility, and comparability of OA grading systems (Pritzker et al., 2006). Based on its prevalence in modern literature, the OARSI grading system is the current gold standard in assessing and comparing OA progression.

OA changes the mechanical properties of articular cartilage. Therefore, correlation is sought between existing metrics for the progression of OA and mechanical properties. Robinson (2016) used a simplified version of the OARSI assessment system to grade 84 cartilage explants. The grades ranged from 0

(healthy) to 4 (eroded). Grades higher than 4 were not tested. Mechanical data were collected for each sample. The data were evaluated using both neo-Hookean and Yeoh models. Parameters were estimated for each sample. Figure 2.2 shows how the ORAIS grade correlates to the shear modulus, as well as other mechanical properties of articular cartilage observed in this study (Robinson et al., 2016).

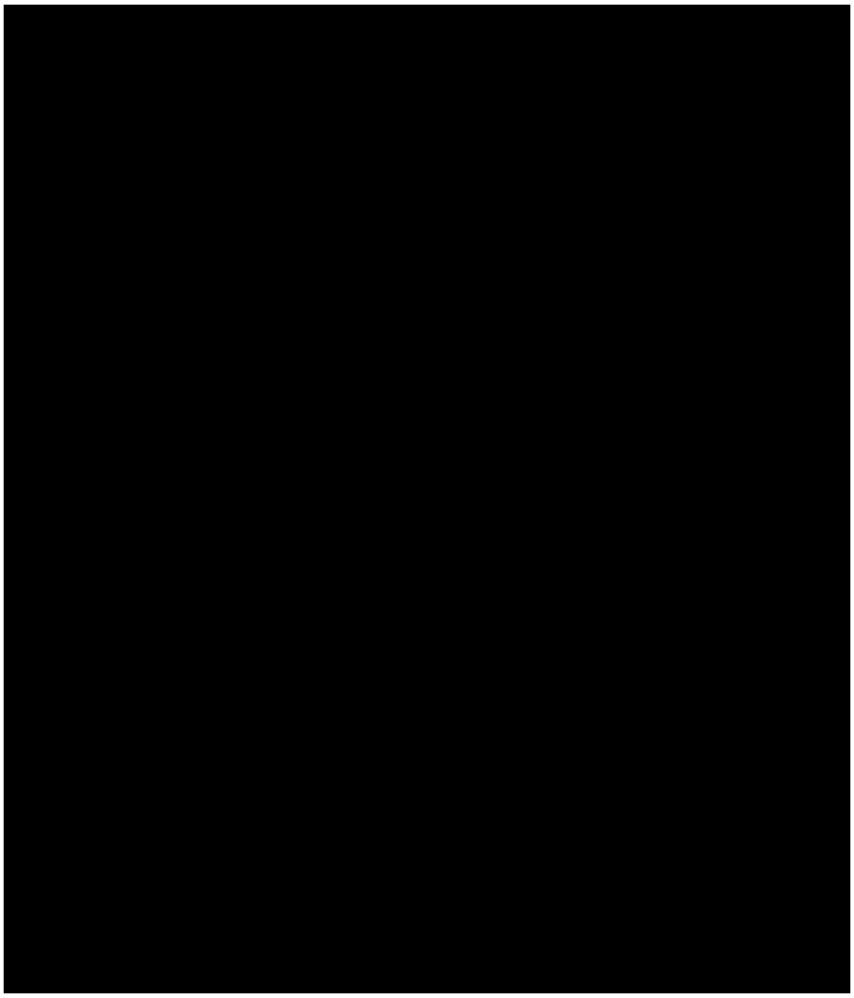

Figure 2.2 *Box and whisper plot from Robinson (2016) that shows how the shear modulus (Y-axis) relates to the OARSI Grade. It provides further information about correlation coefficient (R), significance (p), neo-Hookean model (μ), and Yeoh model (C_{10} and C_{20}). Figure from (Robinson et al., 2016, p. 106)*

Articular cartilage is an anisotropic tissue with discrete regions that have different physiological roles (Sophia Fox et al., 2009). As shown in Figure 1.3, the superficial, middle, and deep zones of articular cartilage have distinct cellularity, cellular morphology, and collagen fiber orientations. The superficial zone of articular cartilage plays a key role in maintaining tissue health (J. Buckwalter & Mankin, 1997; Teeple et al., 2007).

The lamina splendens is an acellular layer at the articular cartilage surface (J. Buckwalter & Mankin, 1997; Fujioka, Aoyama, & Takakuwa, 2013; Rexwinkle et al., 2017). The frictional properties of articular cartilage in guinea pigs were examined using histological methods (Teeple et al., 2007). Gomori trichrome was used to denote subtle thinning and fragmentation of lamina splendens. The damage increased the coefficient for friction when compared to the control, and was thought to be an early sign of OA (Teeple et al., 2007).

Young (2006) studied a functionally similar layer at the articular surface. A glycoprotein layer called proteoglycan 4 (PRG4) protein was identified as a lubricant. This article also references similar terms from other research including “lubricating, superficial zone protein (SZP), megakaryocyte-stimulating factor precursor and camptodactyly-arthropathy-coxavara-pericarditis protein.” This latter protein is produced by superficial zone chondrocytes (Young et al., 2006). The regulation/expression of PRG4 is thought to be important to cartilage health (Young et al., 2006). Disruption of this glycoprotein layer or the chondrocytes ability to produce this protein could have a large effect on cartilage health. One

possibility is changes in biomechanical properties of the articular surface including the shear modulus (Young et al., 2006).

An experiment was conducted to downregulate the expression of PRG4 in a sheep model to test this theory (DuRaine et al., 2009). The results showed significant association with early stage OA degradation, and factors likely involved in the physiological regulation of PRG4 are the anabolic cytokine transforming growth factor-β (TGF-β) and the inflammatory cytokine interleukin-1β (IL-1β). Regulation of PRG4 by TGF-β and IL-1β, and its role in frictional properties of the articular surface was further explored by DuRaine (2009). However, the data showed that the coefficient of friction was not directly influenced by the presence of TGF-β or IL-1β. These conflicting results indicate that PRG4, TGF-β, and IL-1β are not the only factors that may influence the coefficient of friction for articular cartilage, and the multifactorial nature of articular cartilage biomechanical properties.

2.3 Imaging methods

Articular cartilage is not homogeneous (J. Buckwalter & Mankin, 1997). It is anisotropic in terms of collagen fiber orientation, morphology, and composition. Much has been learned about the functional aspects of these traits using different imaging methods (Mark R Buckley, Bergou, Fouchard, Bonassar, & Cohen, 2010; Fujioka et al., 2013). Images of chondrocytes in different zones of articular cartilage have yielded insights into the complex structure of this tissue. Wong (1996) used confocal scanning electron microscopy with a method

of optimizing the fluorescence from the bovine cartilage sample chondrocytes. During preparation the samples were labeled with either [^{3}H]proline or [^{35}S]sulfate, so that during imaging the bioactivity could be measured by the incorporation of either one into the chondrocytes. A stereological method was used to interpret the data collected from one cross-section of the tissue, as if it was 3-dimensional. This allowed for confirmation of the heterogeneous morphology and gave new insight into the bioactivity of chondrocytes in each zone. The deep zone chondrocytes are more rounded when compared to those in the superficial zone, and mainly produce type-2 collagen. Also, the rate that deep zone chondrocytes were synthesizing collagen and proteoglycans was 10 times more than superficial zone chondrocytes. The middle zone is often referred to as the transitional zone, which alludes to sporadic structural traits that are a mix of the deep and superficial zones (M. Wong et al., 1996).

Another method used to elucidate the structural changes between the zones of articular cartilage that also focuses on chondrocytes is digital volumetric imaging (DVI) (Jadin et al., 2005). DVI is a more direct method of producing a 3D representation well suited for a fibrous tissue like articular cartilage (Jaganathan, Tafreshi, & Pourdeyhimi, 2008). This is accomplished using a microtome to produce thin slices of tissue and examining them with an epifluorescent microscope. Jadin (2005) employed DIV methods to measure the cellularity of bovine articular cartilage. The 3D localization of chondrocytes in the cartilage samples was used to create 3D images revealing the proximity of

chondrocyte nuclei to each other as a function of depth. Chondrocyte proximity indicated cell concentration decreased with tissue depth (Jadin et al., 2005).

Chondrocytes can be dyed with fluorescent compounds and imaged with a fluorescent microscope to track displacement in tissue. Buckley (2008) referred to this method as particle image velocimetry (PIV). The prevalence of chondrocytes in articular cartilage allows estimation of the depth dependent shear modulus based on the displacement of chondrocytes at different depths (Mark R. Buckley, Gleghorn, Bonassar, & Cohen, 2008). Buckley (2010) also developed a similar method called grid-resolution automated tissue elastography (GRATE). During tissue preparation for GRATE, a confocal microscope is used to photo-bleach five parallel lines along the z axis each 50 μm apart. The tissue undergoes shear displacement during testing. This causes the photo-bleached lines on the tissue to curve. A custom MATLAB program is used to process the images and calculate displacement as a function of depth a depth. This allows calculation of the shear modulus in the zones off the sample. Buckley (2010) compared the PIV and GRATE methodologies. The displacement and shear modulus measurements were consistent, but GRATE decreased scatter (Mark R Buckley et al., 2010).

The superficial zone of articular cartilage has been of particular interest in imaging studies. There is still debate about different functional and structural attributes of the superficial zone, including further sub-division of this zone in to an additional functional layer, the lamina splendens. Fujioka (2013) referred to the first 6-15 μm of pig articular cartilage as the most superficial zone (MSZ), and

identified three structurally distinct layers therein. A variety of imaging methods were used to gain a comprehensive of view of the MSZ, including histochemical and immunohistochemical methods as well as light microscopy, transmission electron microcopy (TEM) and scanning electron microscopy (SEM) (Fujioka et al., 2013).

Optical coherence tomography (OCT) is an imaging method often used in ophthalmology (Huang et al., 1991). OCT uses interferometer principles, most often with near infrared incident light. This relatively long wavelength allows OCT to image to a greater depth while maintaining resolution. Both 2D and 3D image can be produced from the interferometric data (Huang et al., 1991).

New functional extensions of OCT are being explored that expand its applications. One example is polarization-sensitive optical coherence tomography (PSOCT) (Fan & Yao, 2012). PSOCT uses measurements of the polarization parameters to enhance material characterization, especially in birefringent tissues (including articular cartilage and cardiac tissue). Fan (2012) describes a method built upon other Jones matrix-based algorithms to obtain depth-resolved local retardance (Fan & Yao, 2012). In a later study the same depth-resolved local optical polarization technique and algorithms were used to image the innately birefringent myocardial fibers of a mouse heart (Wang & Yao, 2013). Additionally, an image reconstruction technique called tractography has been used in conjunction with magnetic resonance imaging to visualize the interconnecting structure of neurons. PSOCT imaging data was reconstructed into a tractographic visualization of myocardial fiber organization.

Articular cartilage is also a birefringent tissue, and the fiber orientation and organization are important to its function. Therefore, it is a logical candidate continued application of PSOCT and tractography. Ravanfar (2017) refers to this combination of methods as optical polarization tractograghy (OPT). The study showed OPT to be a valuable tool in the visualization and characterization of collagen fibers in specific zones of articular cartilage (Ravanfar, Pfeiffer, Bozynski, Wang, & Yao, 2017).

2.4 Mechanical Testing

The viscoelastic properties of articular cartilage have been measured using a wide variety of mechanical methods (Neu et al., 2008). One common method is the confined compression test. This method limits confounding variables and allow analyses of the compressive traits for articular cartilage (Torzilli et al., 2006).

Schinagl (1997) cut bovine articular cartilage into 1 cm wide X 4 cm long X 1 cm deep samples, then confined them in a chamber for compression testing. Stepwise compression of tissue at a rate of 0.02% per second was achieved with a computer-controlled stepper motor. A stainless steel filter element allowed for fluid to escape the chamber laterally, but still prevented lateral displacement. The depth-dependent modulus of articular cartilage was visualized and quantified using a compression chamber that worked in conjunction with an epi-fluorescence microscope. The axial displacement of fluorescently dyed chondrocytes at different depth was tracked for 8%, 16%, 24%, and 32%

compression the cartilage thickness. Confined compression tests are ideal for finding the mechanical properties compared to other materials under high controlled circumstances (Schinagl, Gurskis, Chen, & Sah, 1997).

Another highly controlled method of gaining data on the biomechanical properties of articular cartilage is micro-scale mechanical measurement of the tissue using atomic force microscopy (AFM) (Darling et al., 2010; McLeod et al., 2013). AFM is often used to characterize the topography of a surface with very high resolution, but in the case of microscale mechanical testing of cartilage it is used to measure stiffness of the tissue. AFM-based stiffness mapping was used to evaluate how the micromechanical properties of articular cartilage change at different depths (Darling et al., 2010; McLeod et al., 2013). This study confirmed that fiber orientation of collagen contributes to the anisotropic properties and functional distinct regions of articular cartilage.

Many experimental models aim to create an analogous mechanical situation to physiologic conditions of joint articulation. As mentioned previously, the sequence of events during shear load of cartilage is described as follows:

> "Qualitatively, cartilage shear loading resulted in a sequence of 4 events: 1) At the onset of applied lateral displacement, cartilage surfaces initially adhered and began to move laterally in unison. 2) With increasing lateral displacement, lateral deformation and hence E_{xz} increased and occurred throughout the tissue depth. 3) Next, lateral deformation and E_{xz} of cartilage peaked, just as the surfaces detached and slid relative to each

other. 4) With additional lateral displacement, the cartilage deformation and E_{xz} were maintained at a steady-state peak." (B. L. Wong et al., 2008, p. 2069)

In this experiment the samples were loaded into a custom apparatus, that was able to apply a biaxial load (compressive and shear) to the sample. The calcified bone segments of the sample pair were secured while the two articular surfaces were compressed against each other. This means a high frame rate must be used in conjunction with the epifluorescent microscopy setup to capture the moment of peak lateral displacement before detachment at the point of articulation. The objective of this study was to compare shear strain in healthy and degraded tissue with either synovial fluid or PBS acting as the lubricant. They found that shear strain was greatest at the surface (the superficial zone). Also, that there was greater displacement in degraded or less lubricated cartilage (PBS) given the same stress (B. L. Wong et al., 2008).

Two research papers that were previously mentioned for their imaging technique from Dr. Buckley at the University of Rochester, have interesting mechanical testing setups as well. In Buckley 2008 cartilage hemi-cylinders were compressed between two plates to create the necessary axial strain. The tissue was adhered to the plates using cyanoacrylate to prevent detachment of the tissue during lateral displacement. The lateral displacement was created using fine-tuned screws, and a load cell was used to measure the amount of shear force applied. While the tissue was imaged using confocal microscopy after the static axial strain was applied, and then again after the static lateral

force was applied to estimate shear modulus at different depths from the articular surface (Mark R. Buckley et al., 2008). A similar method was used in Buckley 2010 with a couple key changes. First, the lateral displacement force was applied at a sinusoidal rate of 100 Hz with a max displacement of 32 μm at the surface were the tissue is adhered to the shearing plate. Additionally, this study used both PIV and GRATE imaging techniques. Both studies found the shear modulus was significantly higher further from the articular surface (Mark R Buckley et al., 2010).

Chapter 3: Methodology

3.1 Background and Motivation

3.1.1 Imaging studies objectives

The primary objective of this study was to create an effective stage that can image articular cartilage under shear deformation using both fluorescent imaging and optical polarized tractography (OPT). The imaging stage would be able to hold cartilage tissue in order to determine how the orientation of the collagen fibers effect shear modulus at different depths within the tissue. It is theorized that utilizing this imaging methodology, novel data indicative of the structure and function of articular cartilage can be obtained. In order to accurately assess the cartilage using both imaging methodologies, the stage had to be able to address multiple conditions. First, the imaging stage had to be able to create axial displacement of the sample, compressing it to a predetermined percentage of the original thickness. Second, holding the compressive on the tissue, the stage had to be able to apply a perpendicular force along the articular surface of the tissue sample to create a shear deformation. Third, the imaging stage had to be easily integrated into the imaging setup in order to accurately capture the moment of peak displacement during shear deformation. Other characteristics of the imaging stages also had to be changed based on the needs of the imaging methods outline in the next section.

3.2 Fluorescent imaging before detachment/sliding

3.2.1 Imaging Setup

There were many factors that went into creating the initial experimental setup for imaging articular cartilage under shear strain. The first thing to consider was the imaging setup, which was an Olympus Model BX51 fluorescent microscope. The space between the built in mechanical stage and the longest

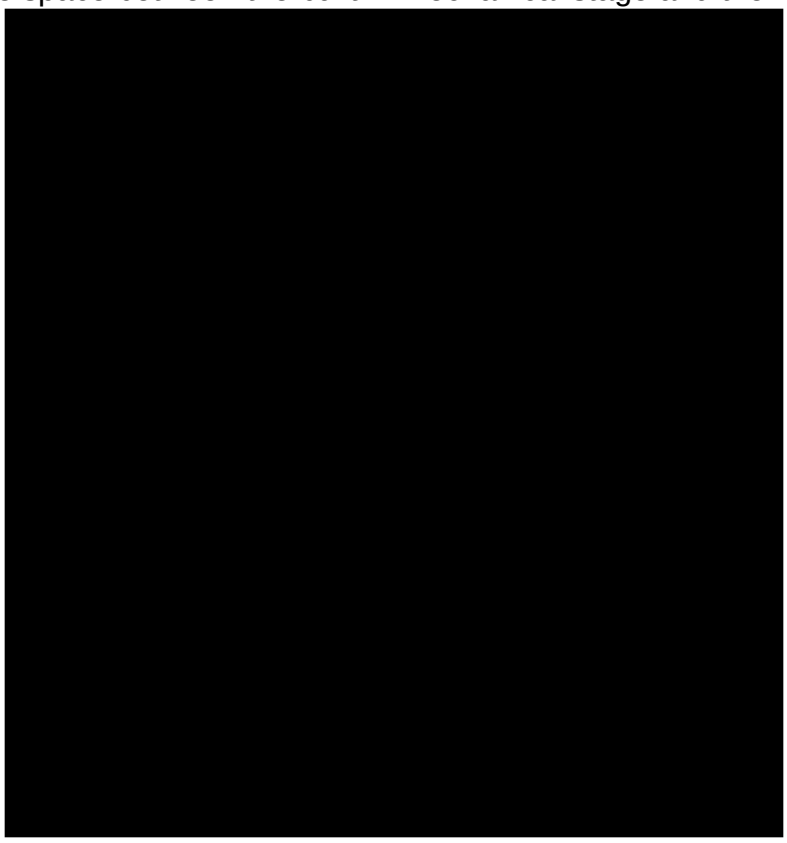

Figure 3.1 *Schematic of the Olympus Model BX51 microscope. (Fluorescence Microscope [Online image]. Retrieved September 12, 2018. https://www.olympus-lifescience.com/en/microscope-resource/primer/techniques/fluorescence/bx51fluorescence)*

objective lens (40X) could be adjusted to be between ~75mm-100mm. A representation of this is shown in Figure 3.1.

The custom apparatus was required to have a height lower than 75mm to ensure it would not interfere with the objective lens. Also, the custom apparatus/stage must have a small footprint to allow for operation of the

microscope during tissue testing. The microscope has screws at the back of the mechanical stage, as shown in Figure 3.2, that allow for the addition of a slide mount. The slide mount, when properly secured with the screws, can be manipulated to change the tissue position under the objective lens during imaging by using the built in vertical and horizontal movement dials. If the apparatus is not too heavy, attachment at this point would allow for easy manipulation of the sample position under the objective.

Figure 3.2 *The mechanical stage from the Olympus Model BX51 with slide mount attached by screws. (Fluorescence Microscope [Online image]. (1919).Retrieved September 12, 2018. https://www.olympus-lifescience.com/en/microscope-resource/primer/techniques/fluoresceence/*

3.2.2 Sample Preparation

The samples were osteochondral explants obtained with IRB approval from patients undergoing total joint replacement. The osteochondral explants were harvested using a 6 mm diameter osteochondral autograft harvester from the condylar surface of the femur or tibia. This is illustrated in Figure 3.3 A and B.

The cylindrical samples had a thickness of 3-5 mm, which includes an average of 2.7mm of articular cartilage and the remainder being calcified bone. The samples were then bifurcated along the axis of the sample using a Buehler Isomet diamond wet saw to create hemi-cylinders (Figure 3.3 C). The flat edge along the axis of the hemi-cylinder displays the superficial zone, medial zone, and deep zone of articular cartilage. This flat must be held perpendicular to the objective lens while undergoing shear deformation (Figure 3.6).

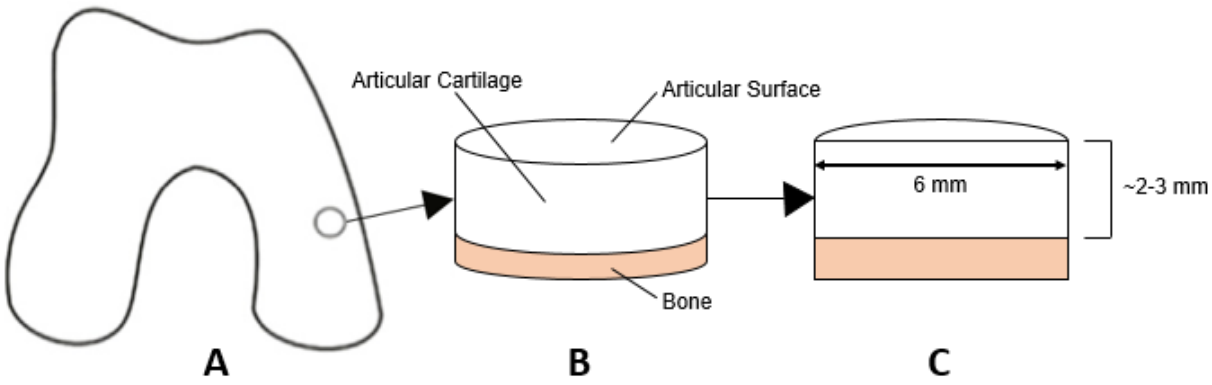

Figure 3.3 *A. The general sampling location that articular cartilage explants were taken from. B. The anatomical areas of the articular cartilage explant. C. Articular cartilage explant after bifurcation with measurements of cartilage thickness (~2-3 mm) and diameter (6 mm).*

Two fluorescent stains were used on the sample; Calcein AM for live chondrocytes, and ethidium homodimer-1 for dead or damaged chondrocytes. Calcein AM is permeable to cell membranes then it has an ester group cleaved by intracellular esterases in only live chondrocytes creating fluorescent dye that is membrane-impermeable ("eBioscience™ Calcein AM Viability Dye," 2016). Ethidium homodimer-1 is membrane-impermeable, but it is able to bind to the DNA of dead chondrocytes ("Ethidium Homodimer-1," 2017). Both fluorophores

have a specific excitation frequencies and emission frequencies, which determine the filter cubes used for excitation and emission capture for each dye. The microscope was setup for efficient change of filter cube to image both dyes. This allows for creation of a composite image.

3.2.3 Apparatus Design

A cylindrical bore with a welled tip (Figure 3.4) was fabricated to properly house the hemi-cylinder articular cartilage explants. The welled tip was designed with the same radius as the sample hemi-spheres, so the samples would sit flush against it. At the top of the well is the sample fixation screw, as shown in Figure 3.4. The screw is inserted in a threaded hole on the welled tip, and the combination is designed to contact the bone perpendicularly on the flat bifurcated side of the sample. The well had to have a depth of 4 mm to accommodate the screw.

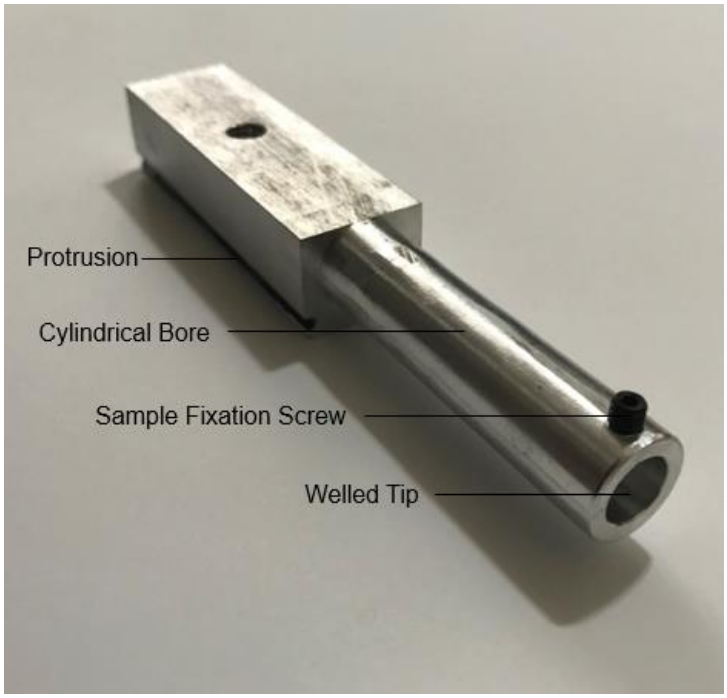

Figure 3.4 *The cylindrical bore used to secure the sample during mechanical testing.*

The cylindrical bore shown in Figure 3.4, has a welded tip. Figure 3.5 shows the welded tip extends from an aluminum block with protrusions that could fit and slide along corresponding recesses that form a track on the Plexiglas base of the imaging stage. The track runs from the center of the base of the imaging stage to the edge, where a micrometer is attached (Starrett Micrometer Head Model 463Mp). The flat face of the micrometer contacted the cylindrical bore with the welded tip, so as the spindle was turned it would progress the bore along the track until it met the shearing surface. Referring to Figure 3.5, the shearing surface is made up of an aluminum block with protrusions that fit and slide along a track running perpendicularly to the track with the cylindrical bore. The micrometer will be used to progress the sample with the articular surface at the forepart at 0.01mm increments until it is compressed against the shearing surface. This creates precise static axial compression of the sample.

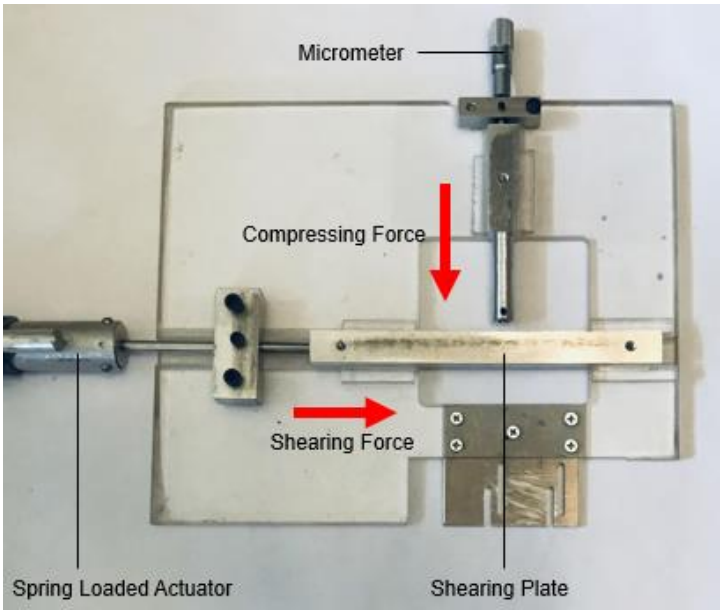

Figure 3.5 *An overview of the apparatus layout.*

The goal for this experimental setup is to rapidly introduce the lateral shear force. The tissue is imaged immediately after the force is introduced to capture the tissue at peak displacement. Once peak displacement is reached

the tissue detaches from the shearing surface and slides back to a relatively static displacement as described in Wong, 2008 in Chapter 2. Figure 3.5 shows the spring loaded actuator used to create this force. The actuator is attached to the base of the apparatus, so when activated it acts on the shearing plate. With the tissue compressed against the shearing surface activation of the actuator results in shearing of the tissue. To quantify the amount of shear force produced the spring actuator is tested using a pendulum. Using the displacement of the pendulum the amount of force can be calculated, and then related to the amount the spring was loaded.

3.2.4 Procedure

The thickness of the cartilage from the articular surface to the calcified bone is measured for each articular cartilage hemi-cylinder using calipers. When preparing to image the articular cartilage samples under shear strain, the testing apparatus had to be attached to the microscope by the two screws that can also be used to hold the slide mount (see Figure 3.2). The images displayed by the Olympus imaging software from the CCD camera are then used to appropriately position the apparatus such that when the sample is introduced it will be under the objective lens shown in Figure 3.6. Then, the aluminum block with the welled tip is removed from its track to position and secure the sample in the well such that the superficial zone, medial zone, and deep zone of articular cartilage all protrude out of the welled tip. Also, the calcified bone section of the sample has to be under the screw threaded through the top, so it can be tightened down to hold the sample in place. With the sample secured, the micrometer is advanced

forward until the sample contacts the shearing surface. Progression is observed on the display or observation tubes. At this point images of the tissue in a relaxed state are taken.

Figure 3.6 *Diagram representing the orientation of the tissue sample to the objective lens. A portion of this image is from Buckley, M. R., et al. (2010). "High-resolution spatial mapping of shear properties in cartilage." Journal of Biomechanics 43(4): 796-800.*

Two images are taken using different filter cubes to promote excitation and capture emissions from both fluorescent dyes. The two images are then made into a composite image. Next, the tissue is compressed to a predetermined fractional strain within physiological load magnitudes, from 10% to 20% relative to its original thickness. The goal is to acquire a composite image of the compressed tissue, but there were issues capturing clear images.

Improvements to the experimental setup that will allow effective imaging are outlined in the discussion section.

Finally, the spring actuator is loaded to produce the appropriate amount of force, which causes shear displacement. Unfortunately, the F-view II CCD camera attached to Olympus Model BX51 did not provide video at sufficient frames per second to capture peak shear displacement. Therefore, no usable images of articular cartilage during peak shear deformation were captured. Improvements to the experimental setup that will allow effective imaging are outlined in the discussion section.

3.3 OPT with Static Shear Load

3.3.1 Imaging Setup

The second round of articular cartilage testing was done using an imaging setup and methods developed by Dr. Gang Yao and Mohammadreza Ravanfar (Ravanfar et al., 2017; Yao et al., 2016). OPT can used to image fiber orientation of a birefringence tissue to show structural changes in human osteoarthritic cartilage (Ravanfar et al., 2017).

OPT requires the sample to remain still during imaging. It is not possible to image articular cartilage at peak displacement under a dynamic load. Therefore, the goal was to create an apparatus that could produce and sustain a consistent shear deformation during imaging.

3.3.2 Sample Preparation

Six cylindrical explants were taken from the condylar surface of a human femur for this imaging study. The cylindrical explants had a diameter of 6 mm, and included a larger portion of bone compared to the previous study with a height ranging from 30-50 mm. A visual representation of the samples is shown in Figure 3.7. The cylindrical explants were then bifurcated into hemi-cylinders using a razor blade with a blade thickness of 0.076 mm. Then, the hemi-cylinders were cut on the calcified bone side. The cuts were made to create relatively uniform overall sample thickness (both bone and cartilage), and a flat surface to fit flush against the bottom of the welled tip. The final result was 6 explants with a height of 8 mm, which were placed in a 10% neutral PBS.

3.3.3 Apparatus Design

The apparatus/imaging stage for the OPT imaging test was designed to hold the sample in place in a 6 mm well at the end of an aluminum block shown in figure 3.7 A. The well had a depth of 5 mm with a screw that threaded down from the top of the well to contact the flat bifurcated surface of the sample. The samples fit flush against the wall of the well, and were held in place by the screw preventing any shifting during imaging. This aluminum block had protrusions that could fit and slide along corresponding recesses. As shown in Figure 3.7, these recesses formed a track that led from one edge of the imaging stage to another track running in a perpendicular direction. The second track housed another aluminum block that would act as the shearing surface during testing. At the end of both tracks are micrometers that progress the flat face forward at 0.01mm increments.

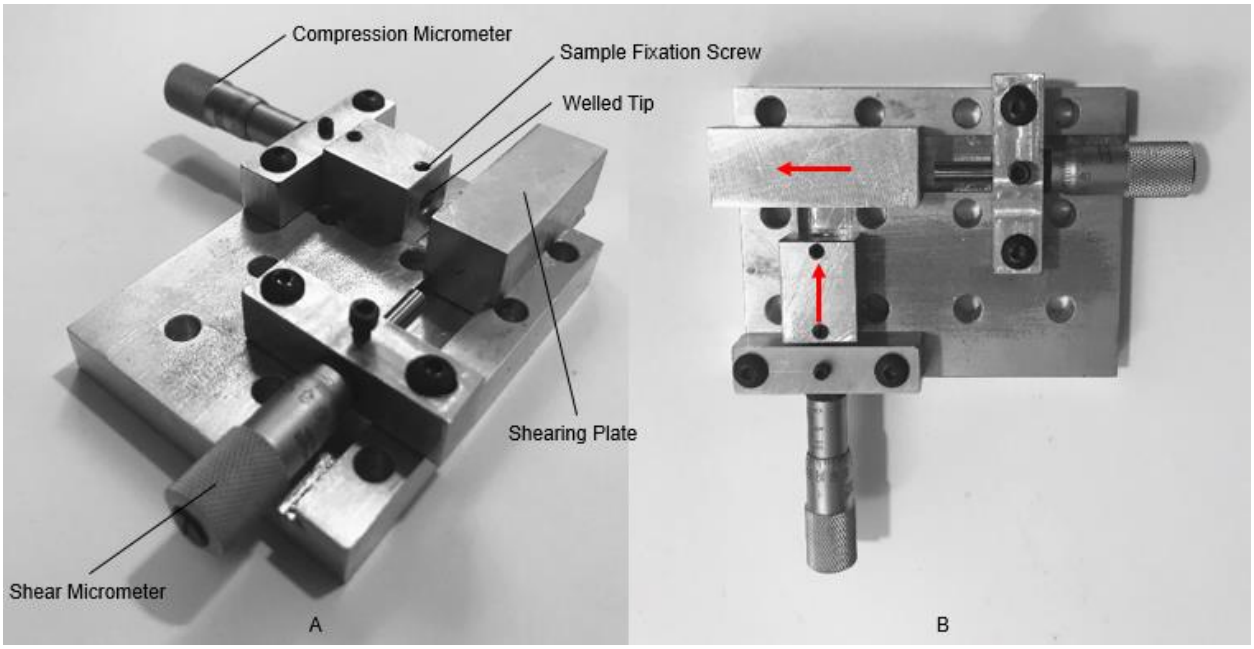

Figure 3.7 *A. Shows a side view of the apparatus with labeled components including the welled tip where the samples are housed. B. An overview of the apparatus with arrows indicating which way the components move to create displacement.*

The compression micrometer loads the sample, and the shear micrometer is progressed to create shear displacement. The samples are adhered to the shear surface to prevent detachment (Mark R. Buckley et al., 2008). The adhesive was 2-Octyl-cyanoacrylate, which has been used on articular cartilage in other work (Hallock, 2001).

3.3.4 Procedure

The sample size was constrained to 2 (n=2) due to the time-consuming process of imaging and reconstruction associated with OPT. Each sample was tested under different conditions to better inform future experimentation and maximize insight into depth specific collagen fiber orientation as it changes under shear strain.

Figure 3.8 shows the sampling location and bifurcation. Before experimentation, each hemi-cylinder sample's overall thickness and cartilage thickness were measured using calipers, representative measurements are shown in Figure 3.8. The amount of axial displacement was calculated based on a percentage of the cartilage thickness shown in Table 3.2. The micrometer was advanced until the welled tip contacted the shearing surface, and the readout on the micrometer was recorded. The micrometer readout at the point the sample contacted the shear surface could be calculated for each sample. This allows for the correct amount of axial displacement to be applied.

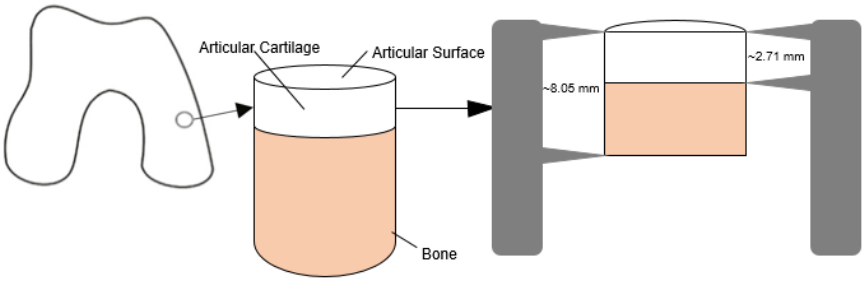

Figure 3.8 *Gives a visual representation of the sampling location, bifurcation and shorting of the sample, and the measurements taken.*

Sample Number	Cartilage Thickness (mm)	Sample Thickness (mm)
1	2.63	8.00
2	2.94	9.60
3	2.77	7.67
4	2.88	7.51
5	2.44	7.87
6	2.58	7.62

Table 3.1 *The sample column lists the sample number from most practical (1) to least (6) for testing. Cartilage thickness was measured for each sample from the tidemark to the articular surface. Sample thickness was measured after preparation for each sample from articular surface to the end of the bone.*

Sample Number	Percent of Cartilage Thickness Compressed (%)	Axial Displacement (mm)	Lateral Displacement (mm)
1	10	0.03	0.20
2	20	0.06	0.40

Table 3.2 *Displays the amount of mechanical strain on corresponding sample number 1 and 2 from Table 3.1.*

The samples in Table 3.1 are order by how suitable they were for this study. *i.e*., how easily each sample could integrated into the imaging stage/apparatus, as well as on general appearance of untarnished articular cartilage (*e.g*. no fibrillation). The “best” two samples were imaged, while the other samples were available if the tissue was damaged or imaging was disrupted.

After bolting the imaging stage/apparatus to the OPT imaging setup to prevent shifting, the compression micrometer (see Figure 3.7) was adjusted so the welled tip was contacting the shear surface. The readout on the micrometer was recorded at this point for displacement calculations. If the values had changed, adjustments to compression and shear values were made. Each sample was loaded into the well and secured by fastening the screw at the top of the well into the calcified bone portion of the sample. The 2-Octyl-cyanoacrylate was lightly brushed onto both the articular surface and the shearing surface. The sample was compressed to the predetermined percentage of articular cartilage thickness shown in Table 3.1 and imaged in a compressed state.

After the first round of imaging was complete the shear strain was applied by advancing the shearing surface a predetermined amount shown in Table 3.2. The amount of lateral displacement was chosen based on previous studies, and to give the most comprehensive look into its effect. Once the desired lateral displacement was achieved using the shear micrometer, the sample is imaged again to show the tissue under shear strain. Both lateral and axial displacement

were maintained in a static state for 15 minutes. The sample was then imaged a third time to show if the tissue had become detached from the shearing surface, and the effect of tissue relaxation while in a sheared state. After imaging a sample the imaging stage/apparatus must be cleaned and reset. The cyanoacrylate is removed from the shear surface by using acetone then wiping it down with saline and allowing it to dry. The data collected from the imaging of the samples was then reconstructed using OPT methods previously described (Ravanfar et al., 2017; Yao et al., 2016).

Chapter 4: Results and Discussion

4.1 Fluorescent imaging before detachment/sliding

The tissue undergoes both compression and shear displacement when using the apparatus for fluorescent imaging before detachment. Integrating the apparatus with the fluorescent microscope allows for control images to be taken prior to displacement. Figure 3.4 and 3.5 show the equipment used for fluorescent imaging before detachment. This apparatus produces the necessary mechanical conditions for testing. However, issues that could not be remedied in the resource environment prevented the collection of useful data. This required a change of research objectives. Nonetheless, the effort is documented here and the apparatus and methodology can be improved and refined in the future (see Chapter 6).

Figure 3.5 illustrates the design executed to accomplish the mechanical objectives, which were to compress the articular cartilage samples, and then exert a shear force along the articular surface. The shear force is introduced by a spring-loaded actuator, which moves the shearing plate shown in figure 3.4. This means there is a high rate of shear loading. The articular surface detaches at the point of peak displacement without the addition of an adhesive or other form of fixation to the shearing surface. It was difficult to capture the moment of peak displacement due to the high rate of loading. This prevented the introduction of shear force in the imaging of the articular cartilage with this imaging setup. A high

frame rate CCD camera may have accomplished the research objective. Please refer to more specific recommendations in Chapter 6.

The fluorescent dye for the live and dead chondrocytes have different emission and excitation frequencies requiring different filter cubes used consecutively to take two images. These images are combined into a composite. Therefore, imaging of both live and dead chondrocytes during rapid loading is not possible. This can be overcome by using one dye, and making changes to settings of the imaging software. This topic is discussed in Chapter 6.

Further testing was performed to discover the testing apparatus's viability if the shear loading issues could be resolved. Specifically, the imaging apparatus's ability to integrate with the fluorescent microscope and capture the tissue under a static compressive load.

The testing apparatus is able to integrate with the microscope. It allows for manipulation of the sample's position under the objective lens without obstructing any of the microscope's function. The sample can be easily imaged, and then precisely compressed by .01mm increments to be imaged again.

However, another issue was encountered in regards to image clarity. When the tissue is compressed the chondrocytes in portions of the sample were no longer visible. Figure 4.1 illustrates the problem. Figure 4.1A shows the control image of the sample contacting the shear surface, but with no compression. Figure 4.1B shows the tissue after compression with large portions of distortion concentrated in the middle of the image. Thus, it was difficult to track displacement throughout the tissue. It should be noted that most

of images taken during the initial experimentation were not retained as they could not be used for PIV. Figure 4.1 were low quality JPEGs kept for reference when discussing the issues and how to proceed, and serve as a rough representation of the issues. In retrospect all images should have been retained to better inform future study.

This difficulty is more problematic due to the anisotropic properties of the articular cartilage. The displacement must be tracked throughout the tissue in order to understand its depth-dependent mechanical traits. Ideally, the full thickness of the sample (from articular surface to the tidemark) should remain in focus during displacement. Therefore, the position of the sample relative to the lens must remain constant.

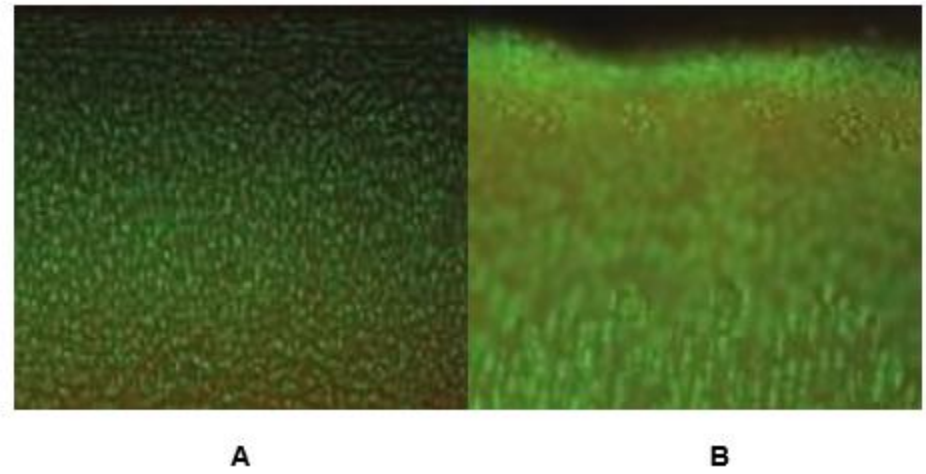

Figure 4.1 *A. Imaged captured using epifluorescent microscope of tissue with no load. B. Imaged captured using epifluorescent microscope of tissue with compressive load.*

The image clarity issue is likely the result of the bifurcated surface being too uneven during compression for the full thickness of the sample to remain in focus. One possibility is that when the compressive load is applied the piece

holding the sample it tips towards or away from the objective lens. Also, lateral displacement during compression could be adding to the uneven imaging surface.

Possible solutions and improvements that would allow attainment of the research objectives are discussed in Chapter 6.

4.2 OPT with Static Shear Load

This study had two samples. Despite the small sample size, the results illustrate the capabilities of the optical polarization tractography technique employed with the testing apparatus developed by Professor Yao's laboratory.

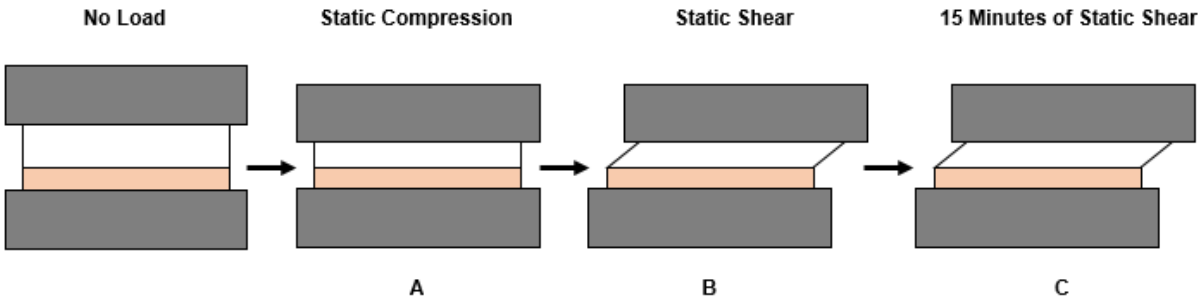

Figure 4.2 *demonstrates the stage of mechanical loading each image (A-C) that corresponds with figure 4.3-4.5. The amounts of displacement are shown in table 3.2.*

Figure 4.3-4.5 show articular cartilage under a static compressive loads and static shear static loads, which supports its usage as a research tool in the future. Table 3.2 show the amount of displacement in S1 and S2. Although there is a limited sample size (n=2) due to limited resources available, which prevented statistically significant results. One thing of particular note when comparing the two samples in Figures 4.3-4.5 is that there is a significantly larger portion of calcified bone in the S2 images comparted to S1 images. This is most apparent

in figure 4.4 S2 a-c at the top where the fiber orientation is randomized and scattered, which is representative of bone.

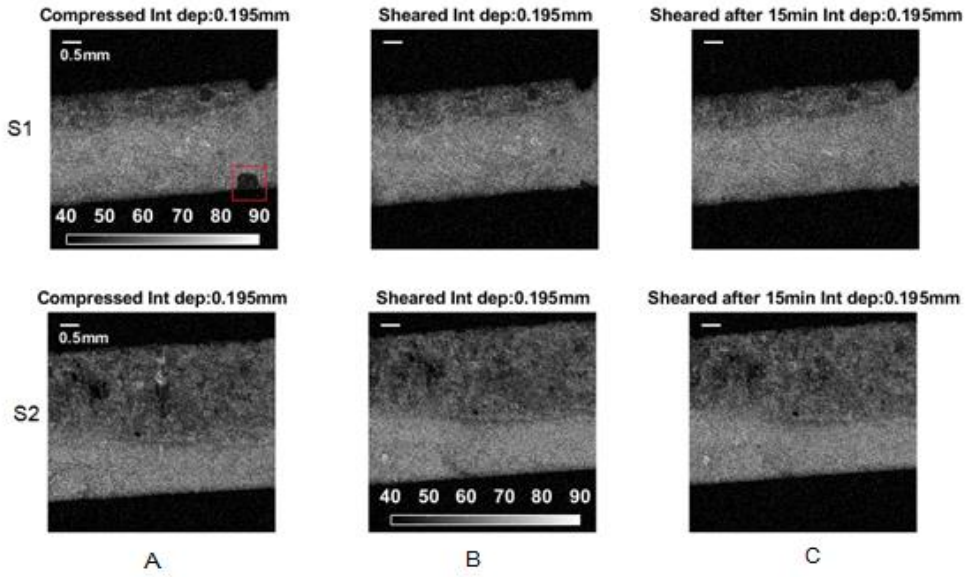

Figure 4.3 Images of S1 and S2 at different stages of mechanical loading (A-C) demonstrated by figure 4.2. These images display intensity in decibels at a depth of ~0.195mm.

In Figure 4.3 there are scattered inconsistences in the intensity, which are to be expected in an inhomogeneous tissue like articular cartilage. There are sections of low intensity in Figure 4.3 at the top of each image, which represent the calcified bone region. At the bottom of the image is the articular surface, which is contacting the shear plate. There are small segment of low intensity along the articular surface giving it a textured appearance. Also, there is one low intensity region (S1 A marked by a red box), which occupies a smaller area in the following images. This could have been caused by the cyanoacrylate used to adhere the tissue to the shearing plate, or possibly damage to the surface. If these low intensity regions/segments are distortions or damage to the tissue it

would likely have an impact on imaging of the fiber orientations (Figure 4.4) and the tractography (Figure 4.5) for these regions.

The images in Figure 4.4 represent the fiber orientation for S1 and S2 under various mechanical conditions. The both 90° and -90° represent fibers that are perpendicular to the articular surface. In S1 there is a clear region approximately where the deep zone should be, and in this region fiber orientation is clearly perpendicular to the surface. S2 has a much smaller region of perpendicularity near the tidemark that signifies the deep zone.

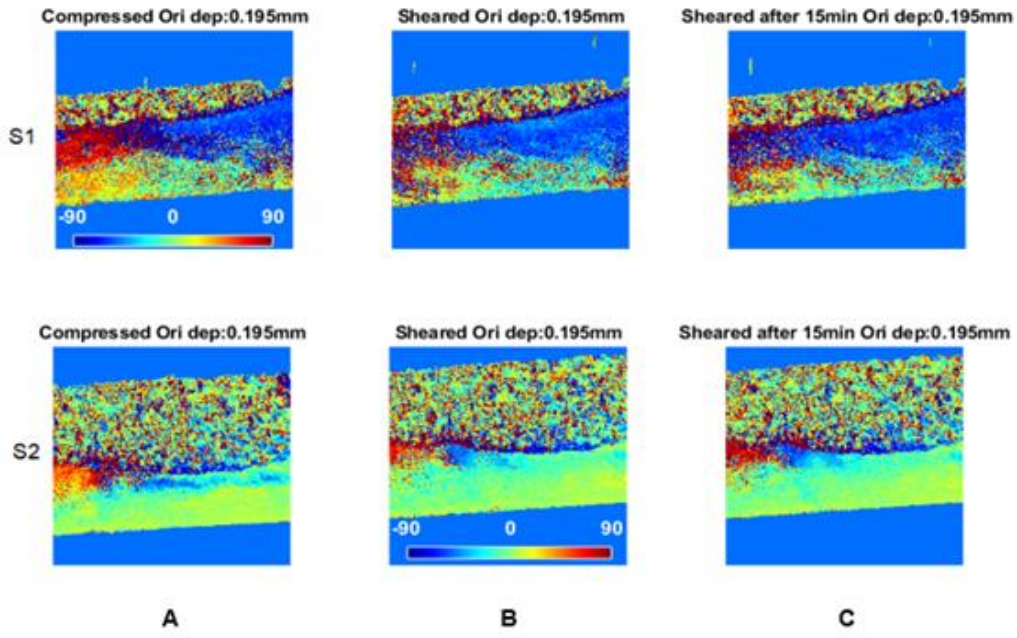

Figure 4.4 *Images of S1 and S2 at different stages of mechanical loading (A-C) demonstrated by figure 4.2. These images show local fiber orientation from -90° to 90°. 0° represent a fiber oriented parallel fiber to the articular surfaces and -90°/90° represent perpendicular to articular surface.*

From figure 4.4 S1 has a region of random fiber orientation progressing (whille moving down the image) to a region of parallel fiber orientation marking both the middle (transitional) zone and superficial zone. In S2 also has a

progression towards parallel fiber orientation, but the middle zone is not as well defined.

There is a noticable change between the images with compression and shear displacement (Figure 4.4) compared to the sample with just compression. Although, there does not appear to be a strong pattern to the fiber orientation change when comparing before and after shear displacement in S2. In S1 there is a slight shift towards more perpendicular fiber orientations likely caused by displacement.

One of the objectives of this experiment was to image the tissue at simulated peak displacement. As the PSOCT system requires 8 minutes to image the tissue the sample had to remain in a static state of simulated peak displacement. Based of previous studies (Wong 2010 and Buckley 2010) the lateral displacement at the shear surface for S1 was 390 μm and for S2 the displacement was 700 μm. To verify that the tissue was not detaching from the shearing plate it was imaged a third time after 15 minutes. When the sheared

image is compared to the sheared “plus 15” image, no noticeable changes were observed. This means the tissue didn’t relax from its laterally displaced state.

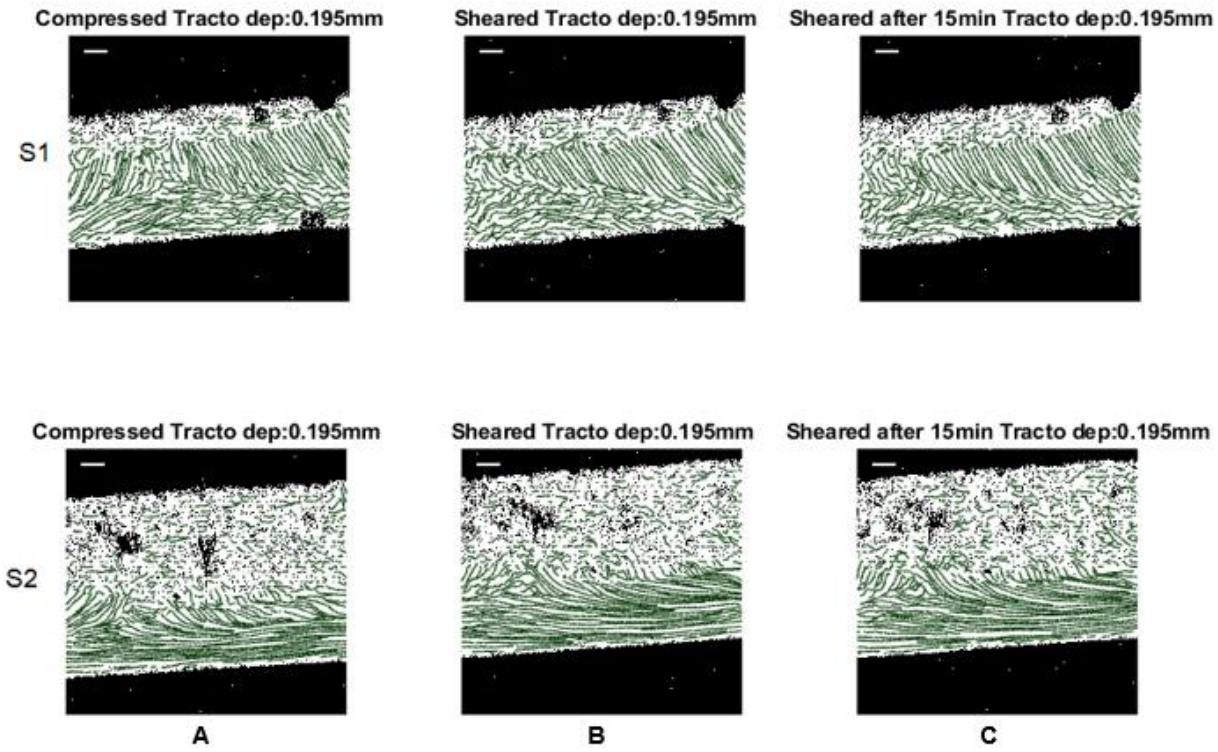

Figure 4.5 *Images of S1 and S2 at different stages of mechanical loading (A-C) demonstrated by figure 4.2. Images generated using a reconstruction method called tractography that represents fiber orientation and organization in different regions of the tissue.*

The tractography representation in Figure 4.5 has some distortions that match up with the sections of low intensity from Figure 4.3. S1 has a larger region of of fibers parallel to the articular surface than was expected. Although, there is a general progression towards parallel fiber orientation closer to the articular surface. In this representation of S1, there is a clear deep zone with fibers oriented perpendicular to the articular surface. In S2 there appears to be a deep zone, but it is harder to distinguish from the bone.

Chapter 5: Conclusions and Recommendations

5.1 Fluorescent imaging before detachment/sliding

There were two main research objectives for this study. First, was to design an apparatus that could integrate with the fluorescent microscope, and create both axial and lateral displacement in a controlled manner. Second, was to use the imaging setup and apparatus to gather data on the anisotropic properties of articular cartilage, and calculate the depth dependent shear modulus. It was discovered that there needed to be modifications to the apparatus to gather the appropriate data.

The fluorescent imaging apparatus and method were not able to accomplish the predetermined research goals. However, with what was learned improvements can be made, and the objectives of this study could be revisited. A refined testing apparatus and methods could result in a valuable research tool that could open up new areas of study.

5.2 OPT with Static Shear Load

The focus of this research was to create an apparatus and method that could be used in conjunction with OPT imaging to image articular cartilage under simulated peak displacement. The apparatus was able to produce the mechanical conditions in the articular cartilage during OPT imaging. However, there were areas that could use additional development to produce better results, which are described in Chapter 6. Further use of this apparatus and

methodology could lead to novel insights into the functional structure of articular cartilage.

The various components of the testing apparatus used in this study successfully preformed their roles. Micrometers were effective at producing a precise amount of compressive and shear displacement, and where able maintain a consistent static load. The 2-Octyl-cyanoacrylate used was able to keep continuous adherence of tissue and shearing over a period of ~30 minutes (two ~8 minute imaging periods and one 15 minute wait period). The combination of the fixations screw and the welded tip secured the sample in position during imaging. The apparatus easily integrated with the OPT imaging setup. Overall, OPT with static shear load apparatus was able to produce the conditions necessary for imaging articular cartilage under simulated peak displacement.

OPT imaging with the static shear load apparatus yielded interesting results. However, the small samples size will require further verification of this testing procedure to ensure its viability. Future applications may provide insight into collagen fiber orientation in articular cartilage and its role in determining the biomechanical properties of the tissue.

Chapter 6: Recommendations

6.1 Fluorescent imaging before detachment/sliding

The apparatus is able to perform some of its functions, but could be improved upon. One of the main attributes of this study in need of revisiting is the ability to capture a high rate of shear loading. This could be accomplished by introducing a high fps CCD camera to the imaging setup.

Once a high fps camera was integrated, it would be useful to have cycles of loading to have multiple opportunities to capture the moment of peak displacement. The cycles would have to be in relatively quick succession to prevent photobleaching. Sinusoidal shear load of the articular cartilage could be used to accomplish this. The sinusoidal loading would still need to create enough displacement to result detachment. This will require an electric actuator that can precisely produce the necessary force/displacement and return to a neutral position at high frequency.

The image clarity issues will require further experimentation and modification to remedy. Using some of the improvements made from the fluorescent imaging apparatus (Figure 3.5) to the OPT apparatus (Figure 3.7) could help limit distortion of the images. Most of these changes came in the form of simplifications. For example, the fluorescent imaging apparatus has a gap in the center of the base resulting in the need for the cylindrical bore (Figure 3.4). The gap was designed to allow the light coming out of the condenser (Figure 3.1) to illuminate the sample. However, this was not necessary as light from the

condenser plays no role in fluorescence, and is not required for positioning the sample under the objective. The smaller portion housing the sample in Figure 3.7 and the minimalized apparatus as a whole would help prevent the sample tipping up during compression.

The image clarity could be improved by confining the flat surface being imaged, while still allowing imaging. One option is using a glass slide over the surface being imaged. However, it would be difficult integrate a slide along the axis and still provide compression and shear at the articular surface. Another possible solution would be to use the previously discussed GRATE method to track displacement. This would require use of a confocal microscope to photobleached lines on the sample, which increases the resources needed for this study. Also, this method is very work intensive. This may have contributed to the limited sample size in Buckley (2010).

After improvements to the testing apparatus are made I believe useful data could be collected. Ideally, the testing apparatus with an epifluorescent microscope could be used to accurately calculate the depth specific and/or collective shear modulus of articular cartilage samples. If this is realized using PIV (rather than GRATE) this relatively fast procedure could make it more viable to use greater sample sizes then other methodologies. The apparatus and method developed here have the potential to be an inexpensive and quick method for biomechanical testing that could then be used to explore other experimental goals.

One possibility for further research is the impact that losing the acellular region of articular cartilage (lamina splendens) has on shear modulus of the tissue as a whole. This could be investigated using the testing apparatus to compare healthy and degraded samples. A method for degrading samples would have to be established. One theoretical option to create this degradation model would be to utilize healthy articular cartilage samples and degrade the articular surface using catabolic enzymes, such as alpha-chymotrypsin, or a fine-tuned mechanical mechanism to breakdown the articular surface in a controlled manner. Then, histological evaluation of the samples could confirm if the appropriate amount of degradation occurred. The testing apparatus could then be used to find the shear modulus of the healthy and degraded samples. Study in this area could provide valuable information on the early detection of OA, and the effect of micro-damage to the cartilages surface on the tissue's biomechanical properties.

6.2 OPT with Static Shear Load

There were issues that could be resolved in the future use of this methodology and apparatus. There may have been too much cyanoacrylate used, which could be why the areas closest to the articular surface were obscured. This is important because the regions closest to the articular surface are of particular interest. A solution to this is to only apply the cyanoacrylate to the shearing surface instead of both the shearing surface and the articular surface. This will require further experimentation to see if the problem persists.

Another possible source of distortion was damage to the articular cartilage samples. Although, this could have been a preexisting condition in these samples, steps can be taken to prevent further damage during sample preparation. For example, the during sample preparation the explants were clamped with locking forceps and split with a razorblade by hand. Using different tools such as a finer blade to bifurcate the samples could prevent any additional damage to the samples.

The use of OPT and the static shear load apparatus could generate information and insight about articular cartilage. This would involve application of the an expanded version of the procedure discussed in Chapter 3 together with some of the changes discussed here to a larger sample size. Different testing conditions could yield interesting results. With a higher sample size and a refined testing conditions there may an increased opportunity for data interpretation. Ravanfar (2017) used different visualization techniques to better understand data from OPT imaging of articular cartilage. One of which was the scatterplot of pixel-wise correlation of parameters, which included fiber orientation (Ravanfar et al., 2017). Using these interpretive tools, more insight could be gained on the shear properties of articular cartilage.

References

Anderson, D. D., Chubinskaya, S., Guilak, F., Martin, J. A., Oegema, T. R., Olson, S. A., & Buckwalter, J. A. (2011). Post-traumatic osteoarthritis: improved understanding and opportunities for early intervention. *Journal of orthopaedic research : official publication of the Orthopaedic Research Society, 29*(6), 802-809. doi:10.1002/jor.21359

Bennett, G. A. (1942). *Changes in the knee joint at various ages: with particular reference to the nature and development of degenerative joint disease*: Commonwealth Fund.

Buckley, M. R., Bergou, A. J., Fouchard, J., Bonassar, L. J., & Cohen, I. (2010). High-resolution spatial mapping of shear properties in cartilage. *Journal of Biomechanics, 43*(4), 796-800.

Buckley, M. R., Gleghorn, J. P., Bonassar, L. J., & Cohen, I. (2008). Mapping the depth dependence of shear properties in articular cartilage. *Journal of Biomechanics, 41*(11), 2430-2437. doi:https://doi.org/10.1016/j.jbiomech.2008.05.021

Buckwalter, J., & Mankin, H. (1997). Articular Cartilage: Part I Tissue Design and Chondrocyte-Matrix Interactions. *JBJS, 79*(4), 600-611.

Buckwalter, J., & Mankin, H. (1998). Articular cartilage: tissue design and chondrocyte-matrix interactions. *Instructional course lectures, 47*, 477-486.

Buckwalter, J. A., Mow, V. C., & Ratcliffe, A. (1994). Restoration of injured or degenerated articular cartilage. *JAAOS-Journal of the American Academy of Orthopaedic Surgeons, 2*(4), 192-201.

Chan, S., Neu, C., Komvopoulos, K., & Reddi, A. (2011). The role of lubricant entrapment at biological interfaces: Reduction of friction and adhesion in articular cartilage. *Journal of Biomechanics, 44*(11), 2015-2020.

Darling, E. M., Wilusz, R. E., Bolognesi, M. P., Zauscher, S., & Guilak, F. (2010). Spatial mapping of the biomechanical properties of the pericellular matrix of articular cartilage measured in situ via atomic force microscopy. *Biophysical Journal, 98*(12), 2848-2856.

Djalalinia, S., Saeedi Moghaddam, S., Moradi-Lakeh, M., Shahraz, S., Naghavi, M., Murray, C. J., . . . Danaei, G. (2017). Prevalence and years lived with disability of 310 diseases and injuries in Iran and its neighboring countries, 1990-2015: findings from Global Burden of Disease Study 2015. *Archives of Iranian medicine, 20*(7), 392-402.

DuRaine, G., Neu, C. P., Chan, S. M. T., Komvopoulos, K., June, R. K., & Reddi, A. H. (2009). Regulation of the friction coefficient of articular cartilage by TGF-β1 and IL-1β. *Journal of Orthopaedic Research, 27*(2), 249-256. doi:10.1002/jor.20713

eBioscience™ Calcein AM Viability Dye. (2016). Retrieved from https://www.thermofisher.com/order/catalog/product/65-0853-39

Ethidium Homodimer-1. (2017). Retrieved from https://www.thermofisher.com/order/catalog/product/E1169

Fan, C., & Yao, G. (2012). Mapping local retardance in birefringent samples using polarization sensitive optical coherence tomography. *Optics Letters, 37*(9), 1415-1417.
Fujioka, R., Aoyama, T., & Takakuwa, T. (2013). The layered structure of the articular surface. *Osteoarthritis and Cartilage, 21*(8), 1092-1098.
Gelse, K., Pöschl, E., & Aigner, T. (2003). Collagens—structure, function, and biosynthesis. *Advanced Drug Delivery Reviews, 55*(12), 1531-1546. doi:https://doi.org/10.1016/j.addr.2003.08.002
Guterl, C. C., Gardner, T. R., Rajan, V., Ahmad, C. S., Hung, C. T., & Ateshian, G. A. (2009). Two-dimensional strain fields on the cross-section of the human patellofemoral joint under physiological loading. *Journal of Biomechanics, 42*(9), 1275-1281. doi:https://doi.org/10.1016/j.jbiomech.2009.03.034
Hallock, G. G. (2001). Expanded applications for octyl-2-cyanoacrylate as a tissue adhesive. *Annals of plastic surgery, 46*(2), 185-189.
Henak, C. R., Anderson, A. E., & Weiss, J. A. (2013). Subject-Specific Analysis of Joint Contact Mechanics: Application to the Study of Osteoarthritis and Surgical Planning. *Journal of Biomechanical Engineering, 135*(2), 021003-021003-021026. doi:10.1115/1.4023386
Huang, D., Swanson, E. A., Lin, C. P., Schuman, J. S., Stinson, W. G., Chang, W., . . . Puliafito, C. A. (1991). Optical coherence tomography. *Science, 254*(5035), 1178-1181.
Hunziker, E. (2002). Articular cartilage repair: basic science and clinical progress. A review of the current status and prospects. *Osteoarthritis and Cartilage, 10*(6), 432-463.
Hwang, H., & Kim, H. (2015). Chondrocyte apoptosis in the pathogenesis of osteoarthritis. *International journal of molecular sciences, 16*(11), 26035-26054.
Jadin, K. D., Wong, B. L., Bae, W. C., Li, K. W., Williamson, A. K., Schumacher, B. L., . . . Sah, R. L. (2005). Depth-varying Density and Organization of Chondrocytes in Immature and Mature Bovine Articular Cartilage Assessed by 3D Imaging and Analysis. *Journal of Histochemistry & Cytochemistry, 53*(9), 1109-1119. doi:10.1369/jhc.4A6511.2005
Jaganathan, S., Tafreshi, H. V., & Pourdeyhimi, B. (2008). A realistic approach for modeling permeability of fibrous media: 3-D imaging coupled with CFD simulation. *Chemical Engineering Science, 63*(1), 244-252.
Julkunen, P., Wilson, W., Isaksson, H., Jurvelin, J. S., Herzog, W., & Korhonen, R. K. (2013). A review of the combination of experimental measurements and fibril-reinforced modeling for investigation of articular cartilage and chondrocyte response to loading. *Computational and mathematical methods in medicine, 2013*.
Lee, T. Q., Gerken, A. P., Glaser, F. E., Kim, W. C., & Anzel, S. H. (1997). Patellofemoral joint kinematics and contact pressures in total knee arthroplasty. *Clinical Orthopaedics and Related Research®, 340*, 257-266.
Lohmander, L. S., Östenberg, A., Englund, M., & Roos, H. (2004). High prevalence of knee osteoarthritis, pain, and functional limitations in female

soccer players twelve years after anterior cruciate ligament injury. *Arthritis & Rheumatism, 50*(10), 3145-3152. doi:10.1002/art.20589
Lorenz, H., Wenz, W., Ivancic, M., Steck, E., & Richter, W. (2004). Early and stable upregulation of collagen type II, collagen type I and YKL40 expression levels in cartilage during early experimental osteoarthritis occurs independent of joint location and histological grading. *Arthritis Res Ther, 7*(1), R156. doi:10.1186/ar1471
Mankin, H. J., & Lippiello, L. (1970). Biochemical and metabolic abnormalities in articular cartilage from osteo-arthritic human hips. *JBJS, 52*(3), 424-434.
Mansfield, J. C., Bell, J. S., & Winlove, C. P. (2015). The micromechanics of the superficial zone of articular cartilage. *Osteoarthritis and Cartilage, 23*(10), 1806-1816.
McLeod, M. A., Wilusz, R. E., & Guilak, F. (2013). Depth-dependent anisotropy of the micromechanical properties of the extracellular and pericellular matrices of articular cartilage evaluated via atomic force microscopy. *Journal of Biomechanics, 46*(3), 586-592.
Meachim, G., Ghadially, F., & Collins, D. (1965). Regressive changes in the superficial layer of human articular cartilage. *Annals of the rheumatic diseases, 24*(1), 23.
Mow, V. C., Ateshian, G. A., & Spilker, R. L. (1993). Biomechanics of Diarthrodial Joints: A Review of Twenty Years of Progress. *Journal of Biomechanical Engineering, 115*(4B), 460-467. doi:10.1115/1.2895525
Mow, V. C., & Guo, X. E. (2002). Mechano-electrochemical properties of articular cartilage: their inhomogeneities and anisotropies. *Annual review of biomedical engineering, 4*(1), 175-209.
Neu, C. P., Komvopoulos, K., & Reddi, A. H. (2008). The interface of functional biotribology and regenerative medicine in synovial joints. *Tissue Engineering Part B: Reviews, 14*(3), 235-247.
Ostergaard, K., Petersen, J., Andersen, C. B., Bendtzen, K., & Salter, D. M. (1997). Histologic/histochemical grading system for osteoarthritic articular cartilage. Reproducibility and validity. *Arthritis & Rheumatism, 40*(10), 1766-1771.
Pond, M., & Nuki, G. (1973). Experimentally-induced osteoarthritis in the dog. *Annals of the rheumatic diseases, 32*(4), 387.
Poole, C. A., Ayad, S., & Schofield, J. R. (1988). Chondrons from articular cartilage: I. Immunolocalization of type VI collagen in the pericellular capsule of isolated canine tibial chondrons. *Journal of Cell Science, 90*(4), 635-643.
Pritzker, K., Gay, S., Jimenez, S., Ostergaard, K., Pelletier, J.-P., Revell, P., . . . Van den Berg, W. (2006). Osteoarthritis cartilage histopathology: grading and staging. *Osteoarthritis and Cartilage, 14*(1), 13-29.
Rasmussen, P. S. (1973). Tibial condylar fractures: impairment of knee joint stability as an indication for surgical treatment. *JBJS, 55*(7), 1331-1350.
Ravanfar, M., Pfeiffer, F. M., Bozynski, C. C., Wang, Y., & Yao, G. (2017). Parametric imaging of collagen structural changes in human osteoarthritic

cartilage using optical polarization tractography. *Journal of Biomedical Optics, 22*(12), 121708.
Rexwinkle, J. T., Hunt, H. K., & Pfeiffer, F. M. (2017). Characterization of the surface and interfacial properties of the lamina splendens. *Frontiers of Mechanical Engineering, 12*(2), 234-252. doi:10.1007/s11465-017-0409-2
Robinson, D. L., Kersh, M. E., Walsh, N. C., Ackland, D. C., de Steiger, R. N., & Pandy, M. G. (2016). Mechanical properties of normal and osteoarthritic human articular cartilage. *Journal of the mechanical behavior of biomedical materials, 61*, 96-109.
Salmon, J. H., Rat, A. C., Sellam, J., Michel, M., Eschard, J. P., Guillemin, F., . . . Fautrel, B. (2016). Economic impact of lower-limb osteoarthritis worldwide: a systematic review of cost-of-illness studies. *Osteoarthritis and Cartilage, 24*(9), 1500-1508. doi:https://doi.org/10.1016/j.joca.2016.03.012
Schinagl, R. M., Gurskis, D., Chen, A. C., & Sah, R. L. (1997). Depth-dependent confined compression modulus of full-thickness bovine articular cartilage. *Journal of Orthopaedic Research, 15*(4), 499-506. doi:10.1002/jor.1100150404
Schmidt, T. A., Gastelum, N. S., Nguyen, Q. T., Schumacher, B. L., & Sah, R. L. (2007). Boundary lubrication of articular cartilage: role of synovial fluid constituents. *Arthritis & Rheumatism, 56*(3), 882-891.
Shenoy, R., Pastides, P. S., & Nathwani, D. (2013). (iii) Biomechanics of the knee and TKR. *Orthopaedics and Trauma, 27*(6), 364-371. doi:https://doi.org/10.1016/j.mporth.2013.10.003
Silverberg, Jesse L., Barrett, Aliyah R., Das, M., Petersen, Poul B., Bonassar, Lawrence J., & Cohen, I. (2014). Structure-Function Relations and Rigidity Percolation in the Shear Properties of Articular Cartilage. *Biophysical Journal, 107*(7), 1721-1730. doi:https://doi.org/10.1016/j.bpj.2014.08.011
Sophia Fox, A. J., Bedi, A., & Rodeo, S. A. (2009). The basic science of articular cartilage: structure, composition, and function. *Sports health, 1*(6), 461-468.
Sun, H. B. (2010). Mechanical loading, cartilage degradation, and arthritis. *Annals of the New York Academy of Sciences, 1211*(1), 37-50. doi:10.1111/j.1749-6632.2010.05808.x
Teeple, E., Fleming, B. C., Mechrefe, A. P., Crisco, J. J., Brady, M. F., & Jay, G. D. (2007). Frictional properties of Hartley guinea pig knees with and without proteolytic disruption of the articular surfaces. *Osteoarthritis and Cartilage, 15*(3), 309-315.
Temenoff, J. S., & Mikos, A. G. (2000). Tissue engineering for regeneration of articular cartilage. *Biomaterials, 21*(5), 431-440.
Torzilli, P. A., Deng, X.-H., & Ramcharan, M. (2006). Effect of Compressive Strain on Cell Viability in Statically Loaded Articular Cartilage. *Biomechanics and Modeling in Mechanobiology, 5*(2), 123. doi:10.1007/s10237-006-0030-5
Vina, E. R., & Kwoh, C. K. (2018). Epidemiology of osteoarthritis: literature update. *Current opinion in rheumatology, 30*(2), 160-167.

Wang, Y., & Yao, G. (2013). Optical tractography of the mouse heart using polarization-sensitive optical coherence tomography. *Biomedical optics express, 4*(11), 2540-2545.

Wong, B. L., Bae, W. C., Chun, J., Gratz, K. R., Lotz, M., & Sah, R. L. (2008). Biomechanics of cartilage articulation: Effects of lubrication and degeneration on shear deformation. *Arthritis & Rheumatism, 58*(7), 2065-2074. doi:10.1002/art.23548

Wong, B. L., & Sah, R. L. (2010). Mechanical asymmetry during articulation of tibial and femoral cartilages: Local and overall compressive and shear deformation and properties. *Journal of Biomechanics, 43*(9), 1689-1695. doi:https://doi.org/10.1016/j.jbiomech.2010.02.035

Wong, M., Wuethrich, P., Eggli, P., & Hunziker, E. (1996). Zone-specific cell biosynthetic activity in mature bovine articular cartilage: A new method using confocal microscopic stereology and quantitative autoradiography. *Journal of Orthopaedic Research, 14*(3), 424-432. doi:10.1002/jor.1100140313

Yao, X., Wang, Y., Ravanfar, M., Pfeiffer, F. M., Duan, D., & Yao, G. (2016). *Nondestructive imaging of fiber structure in articular cartilage using optical polarization tractography*.

Young, A. A., McLennan, S., Smith, M. M., Smith, S. M., Cake, M. A., Read, R. A., . . . Little, C. B. (2006). Proteoglycan 4 downregulation in a sheep meniscectomy model of early osteoarthritis. *Arthritis Research & Therapy, 8*(2), R41-R41. doi:10.1186/ar1898

Zhang, Y., & Jordan, J. M. (2010). Epidemiology of Osteoarthritis. *Clinics in geriatric medicine, 26*(3), 355-369. doi:10.1016/j.cger.2010.03.001